Mapana - Journal of Sciences
2023, Vol. 22, No. 3, *59-79*
ISSN 0975-3303 | https://doi.org/10.12723/mjs.66.3

Adaptive Jellyfish Search Optimization Trained Deep Learning for Breast Cancer Classification Using Histopathological Images

Vijaya P.*

Abstract

One of the most common cancers identified worldwide among women is breast cancer, which has become the foremost reason for death. Due to the complexity of breast tissues, it is essential to accurately detect and classify breast cancer in medical imaging. In this paper, an optimisation-based deep learning technique is created to detect breast cancer using histopathology pictures. At first, the input image taken from the figshare dataset is sent to the pre-processing stage. The median filter is employed at the pre-processing stage to eliminate noise from the input image. Then, the pre-processed images are sent to the segmentation procedure, where the Fuzzy Local Information C-Means (FLICM) technique is used to segment the blood cells. After the segmentation process, feature extraction is carried out. In the feature extraction process, various features, such as area, shape, diameter, and Speeded-Up Robust Features (SURF), are extracted from histopathological images. At last, Deep Q Network (DQN) trained using the developed Adaptive Jelly Fish Search Optimization (AJSO) algorithm is used to identify and classify benign and malignant breast cancer. The devised approach has good accuracy, TPR, and TNR values of 91.1%, 92.1%, and 92%, correspondingly.

* Modern College of Business & Science, Sultanate of Oman; Email: Vijaya.Padmanabha@mcbs.edu.om

Keywords: Breast cancer, Deep learning, median filter, histopathological images, jellyfish search optimisation.

1. Introduction

Cancer, which affects people all over the world on a regular basis, presents a tremendous challenge to medical science. If a patient's cancer is not adequately diagnosed, it can be hazardous since cancer cells multiply quickly over time. Breast cancer is thought to be the second most fatal common cancer, whereas lung cancer is considered the first [2]. As the top cause of mortality in almost every country, cancer has become a significant global problem and concern for people. Tissue cells in the breast alter and divide uncontrollably in the deadly disease known as breast cancer, typically developing a lump [3]. Breast cancer is one of the most prevalent cancers in women around the world, with significant fatality rates. An early detection and treatment of breast cancer patients, according to research, may reduce their mortality rate [10]. The two most frequent varieties of breast tumour are benign and malignant, with benign lesions being those that are not cancerous and are simply cell abnormalities that cannot lead to breast cancer and malignant lesions being those that are cancerous. In order to effectively treat the disease, early identification of breast cancer [15] [16] is seen to be a crucial responsibility. In order to detect numerous diseases, pathology is a more precise and efficient method. Breast cancer is discovered utilizing a computer-assisted diagnostic (CAD) system and histopathological images [11]. Histopathology is the practice of microscopic examination and in-depth analysis of a biopsy sample carried out by a specialist/pathologist to research cancer growth in the organs [14]. The histopathological examination has long been held in high esteem as the gold standard for detecting breast cancer since it has unrivalled authority when compared to other examination methods. Both the visual analysis and the physical interpretation of historical photographs require time. Hence, in the modern day, automatic diagnosing techniques are required. By lessening their workload and delivering more accurate results, they may be beneficial for radiologists, pathologists, and other specialists [12]. The CAD categorization of breast cancer histological images is anticipated to ease pathologists' heavy burden and enhance the precision and effectiveness of pathological investigations, which

have significant clinical value and social relevance [3]. Deep learning algorithms have produced outstanding results in medical diagnosis and image analysis, in addition to their contributions to breakthroughs in a number of fields like drug development, time-series modelling, and optimisation methods. Deep learning algorithms have found success in the detection of breast cancer using digital histopathology pictures [4]. This method aids clinicians in making more comfortable and accurate diagnoses of disease [2].

This study introduces the classification of breast cancer using histopathological pictures from the AJSO-DQN. The classification method involves the pre-processing, segmentation of blood cells, feature extraction, and categorization of breast cancer. Here, the input data is acquired first. When the data has been acquired, the median filter is used for pre-processing. Following pre-processing, FLICM is used to segment blood cells. The feature extraction is accomplished on segmented input histopathological images, where various features, such as shape feature, like, area, shape, and diameter, and SURF are extracted. Following their classification into benign and malignant breast cancer using DQN, which was trained using the AJSO algorithmic technique, the extracted features are sent for the detection of blood cancer based on the severity grades.

The investigation's main impact is outlined below;

- ***Established AJSO_DQN for breast cancer classification:*** Utilizing histopathological pictures, a technique, named AJSO_DQN is developed for classifying breast cancer. The FLICM is employed in this instance for blood cell segmentation. Furthermore, the suggested AJSO is used to train the DQN. The developed AJSO combines JSO and the adaptive notion.

In this work, the remaining work is structured as follows: Section 2 analyses the literature study; Section 3 describes established AJSO_DQN; Section 4 examines discussion and outcomes; and Section 5 examines the conclusion.

2. Literature Survey

The second-leading cause of death for women worldwide is breast cancer. Several methods have been created in an effort to produce

quick and accurate breast cancer prediction tools, but it appears that misclassifications are caused by the resemblance between benign and malignant types. This inspired the development of a novel technique for categorizing breast cancer using histopathology images. Some of the traditional breast cancer classification works are discussed below. Mohanakurup, V., *et al.* [1], developed an efficient method named Composite Dilated Backbone Network (CDBN) for breast cancer diagnosis. For early breast cancer analysis, this method was less expensive and more effective. Inaccurate categorization occurred because histology scans of breast tumours lacked label information. Ahmad, N., et al. [2] introduced Transfer learning (TL) to classify histopathological images for breast cancer diagnosis. This method was more accurate and less complex. However, the patch selection methodology was not applied in this method's other medical imaging-related activities. Zou, Y., et al. [3], established Attention High-Order Deep Network (AHoNet) for the classification task of breast cancer histopathological images. Here, the method's suitability for the medical image categorization task was validated. It did not take into account how high-order statistical models and attention mechanisms would affect this medical task. Burcak, K.C., et al. [4] developed Machine learning -based Deep Convolutional Neural Network (HCNN) model for automatic detection and classification of breast cancer. This strategy reduced decision-making time by enhancing pathologic diagnosis accuracy. Yet, the process was quite complicated.

3. Proposed Method

This research's main objective is to create a system for categorizing breast cancer. Firstly, the input image data acquired from the database is allowed for pre-processing using the median filter [5] to de-noise the naturally occurring noise in the input histopathological images. The pre-processed input images are forwarded to the segmentation process to segment the blood cells using FLICM algorithm [6]. Feature extraction is performed on the segmented input histopathological images, where various features, such as shape feature, like, area, shape, and diameter, and SURF [7] is extracted from the histopathological images. The extracted features are forwarded for the detection of blood cancer based on the severity grades and are classified into benign and malignant breast cancer

using DQN [8], which is trained using the developed AJSO algorithmic technique. The AJSO is the integration of adaptive concept and JSO [9]. Adenosis, fibroadenoma, phyllodes tumour, and tubular adenoma are the four types of benign breast cancer, whereas carcinoma, lobular carcinoma, mucinous carcinoma, and papillary carcinoma are the four types of malignant breast cancer. Figure 1 represents the block diagram of the proposed AJSO-DQN technique for the organization of breast cancer using Histopathological images.

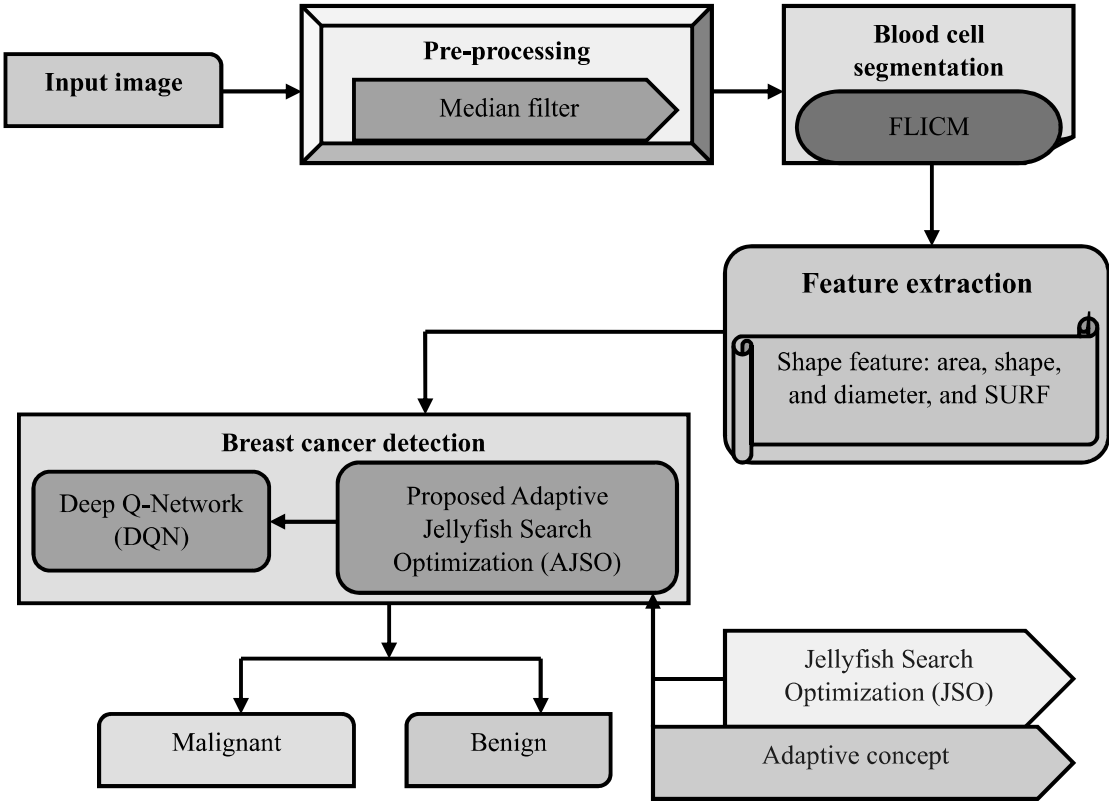

Figure 1. Block diagram for the proposed AJSO-DQN method for identifying breast cancer from Histopathological pictures

3.1 Data acquisition

The first step in the process is data collecting, during which the histopathological pictures of breast cancer are selected from a ξ dataset.

$$\xi = \{G_1, G_2, ..., G_z, ..., G_a\} \quad (1)$$

Wherein, total images extant in ξ dataset is illustrated as *a*, and G_Z indicates the z^{th} image.

3.2 Pre-Processing Using Median Filter

In order to forecast the important noise in the image and remove the unnecessary noise, it is done during the pre-processing stage. The median filter is used in this instance for pre-processing. Median filter input is in pre-processing.A median filter is used depending on the thresholding value to eliminate noise.The median filter [9] evaluates pixel size in a certain region and removes the median as the newer value of the domain's center pixel from the domain. It not only removes or minimizes ambient noise and pulse disturbance, but it also keeps information at image boundaries. The median filter can be expressed by,

$$\delta_e = \hat{\varsigma}(v,d) = median\left\{z(v,d),(v,d) \in \varphi_{vd}\right\} \qquad (2)$$

Here, *z(v,d)* is indicated as noise, and the output pixel value of the filtering consequence is denoted as $\hat{\varsigma}(v,d)$which is the preparation average value, and the filtered picture is signified as δ_e.

3.3 Blood cell segmentation

The blood cell segmentation uses a pre-processed image δ_e as an input. FLICM [6] is used here to segment blood cells. FLICM uses the fuzzy factor ω_{mv} for the following purposes:

a) to protect sturdiness and noise insensitiveness, it integrates local spatial and local grey level information in a fuzzy way.

b) to manage the power of the neighbourhood pixels based on their distance from the middle pixel.

c) to utilize the original image for preserving all details.

d) to be free of every parameter selection.

By using the fuzzy factor, FLICM includes local spatial and gray level information into its objective function, described in terms of

$$\rho_g = \sum_{w=1}^{\lambda}\sum_{m=1}^{v}\left[N_{mw}^{g} \parallel L_w - y_m \parallel^2 + \omega_{mw}\right] \qquad (3)$$

The two conditions that must be met for ρ_g to be at its local negligible dangerous with regard to N_{mw} and y_m are as follows:

$$N_{mw} = \frac{1}{\sum_{s=1}^{v}\left[\frac{\|L_w - y_m\|^2 + \omega_{mw}}{\|L_w - y_m\|^2 + \omega_{sw}}\right]^{\frac{1}{g-1}}} \quad (4)$$

$$y_m = \frac{\sum_{w=1}^{\lambda} N_{mw}^{g} L_w}{\sum_{w=1}^{\lambda} N_{mw}^{g}} \quad (5)$$

Wherein, ω_{mw} indicates fuzzy factor where the local window's w^{th} pixel marks its centre, reference cluster is represented as m, N_{mw} represents the w^{th} pixel's level of cluster membership in the m^{th} cluster, on each fuzzy membership, g is the weighting exponent, and the centre of cluster m^{th} prototype is called y_m. In FLICM, initially, cluster prototypes, stoping criteria, and the fuzzification parameters are set. Then, the fuzzy partition matrix *(M)* is initialized randomly and the loop counter *(l=0)* is set. Afterthat, the cluster prototypes are calculated using equation (5) and the membership values are calculated using equation (4). If, $\{M^l - M^{l+1}\} <$ *stopping criteria*, then stop the process, otherwise, set $l=l+1$ and repeat the above processes.

The output $\delta_s$of blood cell segmentation is forwarded to the feature extraction phase.

3.4 Feature extraction

For precise and successful illness diagnosis and classification, the majority of image processing programs view feature extraction as a crucial component. The segmented blood cell δ_s is fed input of the feature extraction process. In this process, the features like SURF, area, shape and diameter are extracted.

i) SURF: One of the best methods suitable for real-time applications is the "SURF" [7] algorithm, which is regarded as a reliable local feature detector and extractor algorithm. It has a wide range of uses in computer vision, such as 3D reconstruction and object recognition. An integral image is an image with each point equal to η in this image *(h,l)* keeps total number of pixels in the input image τ in a rectangle created by the origin and η , as shown in equation(6);

$$\tau(\eta) = \sum_{n=0}^{n\leq h} \sum_{d=0}^{d\leq l} \tau\,(n,d) \qquad (6)$$

In equation (7), it is stated what the Hessian matrix $U(\eta,\mu)$ in η at scale is:

$$U(\eta,\mu) = \begin{bmatrix} W_{hh}(h,\mu) & W_{hl}(h,\mu) \\ W_{lh}(h,\mu) & W_{ll}(h,\mu) \end{bmatrix} \qquad (7)$$

Here, the second order derivation of the Gaussian filter with the picture at point η produces $W_{hh}(h,\mu)$ and $W_{ll}(h,\mu)$. In order to maximize computational effectiveness, the weights applied to the rectangular regions are kept simple.

$$\det\left(U_{app}\right) = \varepsilon_{hh}\varepsilon_{ll} - (M\varepsilon_{hl})^2 \qquad (8)$$

Here, *M* indicates the filter response's relative weight and it is given by the following expression,

$$M = \frac{\|W_{hl}(1,2)\|P\|\varepsilon_{ll}(9)\|P}{\|W_{ll}(1,2)\|P\|\varepsilon_{hl}(9)\|P} \qquad (9)$$

In order to maintain the Hessian determination process's equilibrium, the relative weight of the filter *M* is used in this calculation. The SURF is represented as λ_1.

ii) Area: The area feature, represented by λ_2, is calculated by enumerating pixels in the image.

iii) Shape: It is a significant characteristic in cancer classification and is also known as compactness. The shape feature is represented by λ_3.

iv) Diameter: The number of pixels that exist from one location along the boundary to another point across from it in the boundary to the centre of the segmented region is used to quantify this property, which is designated as λ_4 .

Various texture-oriented structures are combined to form a feature trajectory, which is defined as,

$$\beta = \{\lambda_1, \lambda_2, \lambda_3, \lambda_4\} \quad (10)$$

Wherein, a feature vector is signified as β.

3.5 Breast cancer detection using AJSO_DQN

The breast cancer is detected after the feature extraction process by using DQN [8]. The recognition of breast cancer now uses feature vector output. The DQN, which is trained by the suggested AJSO algorithm and newly integrated by the integration of Adaptive concept and JSO [9], detects breast cancer.

3.5.1 Architecture of DQN

DQN [8] is one of the most frequently used reinforcement learning techniques, and it uses CNN to estimate the action-value function known as the Q-function. In a compact manner, DQN represents both high-dimensional images and Q-function. Furthermore, DQN makes use of experience replay. The experience replay is performed by storing the agent's experiences $K_Z = (F_Z, I_Z, J_Z, F_{Z+1})$ at every time step z in a database $\gamma_{Qnet} = \{k_1, \ldots\ldots, k_z\}$. The data set γ_{Qnet} is referred to as replay memory. At the time of learning process, the Q-learning updates are performed on sample of experiences. The Q-learning updates at iteration uses the below loss function:

$$D_b(\theta_b) = Y[F + \varphi max\hat{\alpha}(k, I; \theta_b^-) - \alpha(k, I; \theta_b)^2] \quad (11)$$

Here, reward is signified as F, discount factor is symbolized as φ, θ_b indicates network constraints of at b iteration, θ_b^- is one of the network characteristics used to calculate the target at iteration b. It is the foundation for using aim of the network in DQN, and ξ_a is DQN result. Figure 2 shows the structural view of DQN.

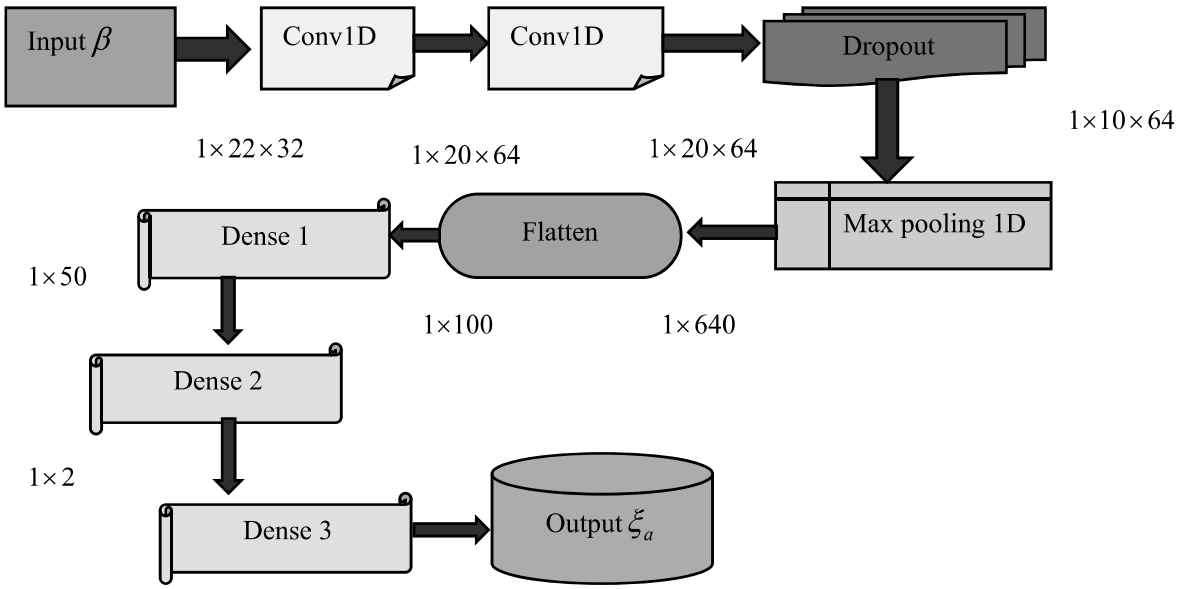

Figure 2. Architecture of DQN

3.5.2 Proposed AJSO

For the purpose of optimally selecting the weights of the DQN classifier, the AJSO is designed in this part. The application of the adaptive notion allows the classifier to change its knowledge rate as it becomes proficient, increasing competence. The JSO [9]is a bio-inspired metaheuristic algorithm based on jellyfish food-finding behaviour in the ocean. In order to find places that give prospective perfect positions for locating food, exploration is more likely than exploitation. Over time, however, exploitation is more likely, and the jellyfish choose the best location within the examined areas. According to analytical results, JSO is employed in various fields, including power schemes and liveliness groups, networking and communication, civil and construction engineering, estimate, categorization, and artificial intelligence optimisation. The AJSO is created by integrating the JSO with the adaptive concept in order to identify the root causes of the inability to precisely identify the best course of action in every circumstance. Hence, hybridized Adaptive principle, and JSO offered superior training outcomes. Below are the mathematical stages for the proposed AJSO.

Step i) Initialization: Typically, a random initialisation process is used to populate an artificial optimisation algorithm. The logistic map is a chaotic map used by JSO to increase initial population diversity while maintaining training simplicity. Compared to random selection, it produces more diversified starting populations and is less likely to have early convergence, as seen in equation (12).

$$H_{v+1} = fH_v(1 - H_v), 0 \leq H \leq 1 \qquad (12)$$

Here, H_{v+1} indicates the location of v^{th} jellyfish, H_V represents the logistic chaotic value of where the v^{th} jellyfish is located, and parameter *f* is set to 4.0.

Step ii) Fitness function: Although issue is accessible as a discounttricky, the fitness metric taken into account in this circumstance is MSE, which is offered by,

$$\varsigma = \frac{1}{v}\sum_a^v(\xi_a^* - \xi_a)^2 \qquad (13)$$

Here, whole set of count sample signified as v, target output is indicated as ξ_a^*, and result of DQN is represented as ξ_a .

Step iii) Determination of ocean current: The ocean circulation contains a huge number of nutrients, which makes jellyfish sensitive to it. Equation (14) provides the new location of each jellyfish.

$$H_v(\partial + 1) = H_v(\partial) + rand(0,1) \times \overrightarrow{td} \qquad (14)$$

For making *rand* as self-adaptive, the following expression is used.

$$rand = \left[1 - \frac{\partial}{max}\right](\varpi \times B_0) \times \sigma \qquad (15)$$

Here, $H_v(\delta + 1)$ represents jellyfish's new location, jellyfish's current location is signified as $H_v(\delta)$, B_0 represents constant set to 0.5, the value of σ is 0.1 and rand is made adaptive.

Step iv) Evaluate Jellyfish swarm: Both passive (type A) and active (type B) movements of jellyfish in swarms are possible. Initially, when a swarm is just starting to develop, the majority of jellyfish exhibit type A motility. Over time, they start to behave more and more like type B creatures. Jellyfish move in a type A motion as they circle their own areas. Equation (16), provides the updated coordinates for each jellyfish.

$$H_v(\delta + 1) = H_v(\delta) + t \times rand(0,1) \times (B_u - B_l) \qquad (16)$$

Here, B_u and B_l represents upper bound and lower bound onlookup box, motion coefficient is indicated as $t>0$.

Step iv) Mechanism of time control: Jellyfish that are part of a swarm switch between type A and type B schedules. Early predilection is assumed to type A, but as time goes on, kind B gains favour.

$$j(\partial) = \left| \left(1 - \frac{\partial}{\max}\right) \times (2 \times rand(0,1) - 1) \right| \qquad (17)$$

Here, time control function is denoted as $j(\partial)$, time is indicated as ∂, and max signifies the total number of iterations.

Step v) Re-evaluate the fitness: The updated solution with the lowest fitness is determined to be the best one by evaluating the fitness function of the updated solution.

Step vi) Termination: Till the ideal answer is found, iteration is continued. Once the best option has been found, the iteration process is over. The pseudocode for the developed AJSO method is shown in Algorithm 1.

Algorithm 1. Algorithmic steps of AJSO

Input: size of population

Adjust population of jellyfish H_v using muddled map

Analyze quantity of food at each H_v

Identify the jellyfish at the area that has the most food right now

For $\partial = 1$

    Calculate the time control $j(\partial)$ using equation (17)

If $\boldsymbol{j(\partial) \geq j_0}$

Ocean current is followed by jellyfish

        Find ocean current

The jellyfish's new position is revealed by using equation (14)
Else
Within a swarm, jellyfish migrate
If rand (0,1)>(1-$j(\partial)$)
Jellyfish move in a type A manner (passive motion) using equation (16)
Else
Type B motion is displayed by jellyfish (active motion)
End if
End for
Determine if the boundary criteria are met and estimate how much food was available at the new location.
Compute quantity of food at the new location
End for

Output: The best solution

As a result, the hybridization of the adaptive concept and JSO successfully achieved the stability of an ideal solution.

4. Results and Discussion

The presented AJSO_DQN results are described in this section using performance measures.

4.1 Experimental set-up

Investigating AJSO_DQN is done with the PYTHON tool.

4.2 Experimental results

Figure 3 displays the experimental outcomes of the AJSO_DQN for breast cancer classification. Figure 3a) displays the input image, while Figures 3b), 3c), 3d), and 3e) represent the pre-processed, segmented, SURF feature, and classified images, respectively.

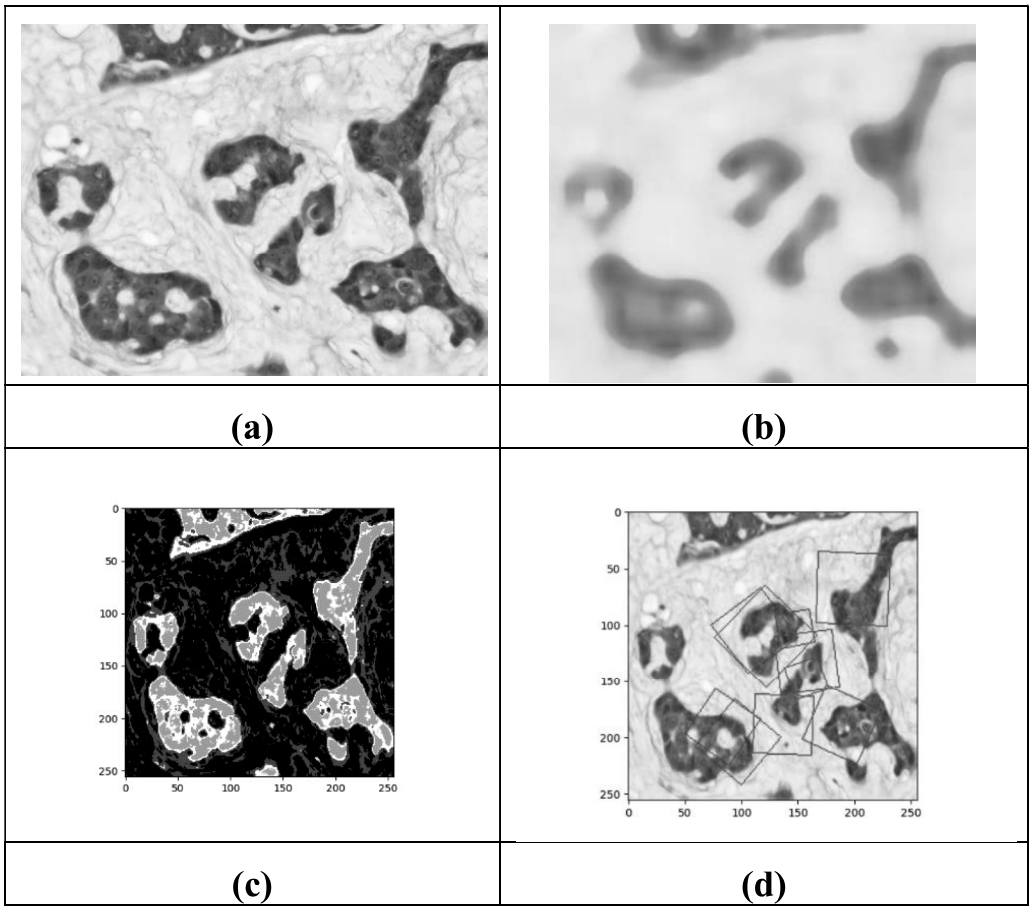

Figure 3. Experimental results of AJSO_DQN a), b) represents the input and pre-processed image, c), d) indicates segmented and SURF image

4.3 Dataset description

The figshare dataset [13] is used for the investigation of the introduced AJSO_DQN. There are three types of brain tumour represented by 3064 T1-weighted contrast-enhanced images in this brain tumour dataset. The readme file contains information about the dataset in great detail.

4.4 Evaluation metrics

The effectiveness of a recently presented AJSO_DQN is investigated using performance indicators like accuracy, TPR, and TNR.

4.4.1 TPR:

TPR estimates the number of positive examples that were appropriately recognized out of the multitude of positive examples. Equation (18) is used to calculate it.

$$TPR = \frac{\pi_p}{\pi_p + S_n} \quad (18)$$

Here, represents true positive, false negative is designated as S_n.

4.4.2 TNR:
The percentage of incorrectly identified negative samples divided by the total number of negative samples is used to compute it.

$$TNR = \frac{\pi_n}{\pi_n + S_p} \quad (19)$$

Wherein, S_p illustrated as false positive, and true negative is indicated π_n.

4.4.3 Accuracy:
The percentage of samples that have been correctly identified across the board serves as the unit of accuracy. Below is the expression for accuracy;

$$Accuracy = \frac{\pi_p + \pi_n}{\pi_p + \pi_n + S_p + S_n} \quad (20)$$

4.5 Comparative methods

The performance of the AJSO_DQN developed for breast cancer classification is accessed in comparison to that of other detection techniques including CDBN [1], Transfer learning [2], AHoNet [3], and DCNN [4].

4.6 Comparative assessment

Breast cancer images from the figshare dataset are used to evaluate the AJSO_DQN, which takes into consideration different counts of the k-fold and training data percentages depending on various evaluation metrics.

4.6.1 Assessment considering K-fold

By increasing the value of k-fold from 5 to 9, Figure 4 illustrates how the produced AJSO_DQN is compared to performance measurements. Figure 4a) shows the accuracy test. In comparison to standard approaches like CDBN, Transfer learning, AHoNet, and DCNN, the accuracy achieved by the suggested method when the K-fold value is 9 is 0.917 as opposed to 0.799, 0.827, 0.882, and 0.892 for each of the four methods, respectively. Figure 4b) illustrates the assessment of the AJSO_DQN in respect to TPR. Here, on the off chance that the worth of K-fold is 9, the TPR of the proposed strategy is 0.921, while ordinary procedures, as CDBN is 0.791, Move learning is 0.850, AHoNet is 0.869, and DCNN is 0.879 individually. Figure 4(c) depicts the TNR valuation. The developed method has a TNR of 0.911 when the value of K-fold is 9, whereas conventional methods like CDBN, Transfer learning, AHoNet, and DCNN have TNRs of 0.799, 0.825, 0.879, and 0.886, respectively.

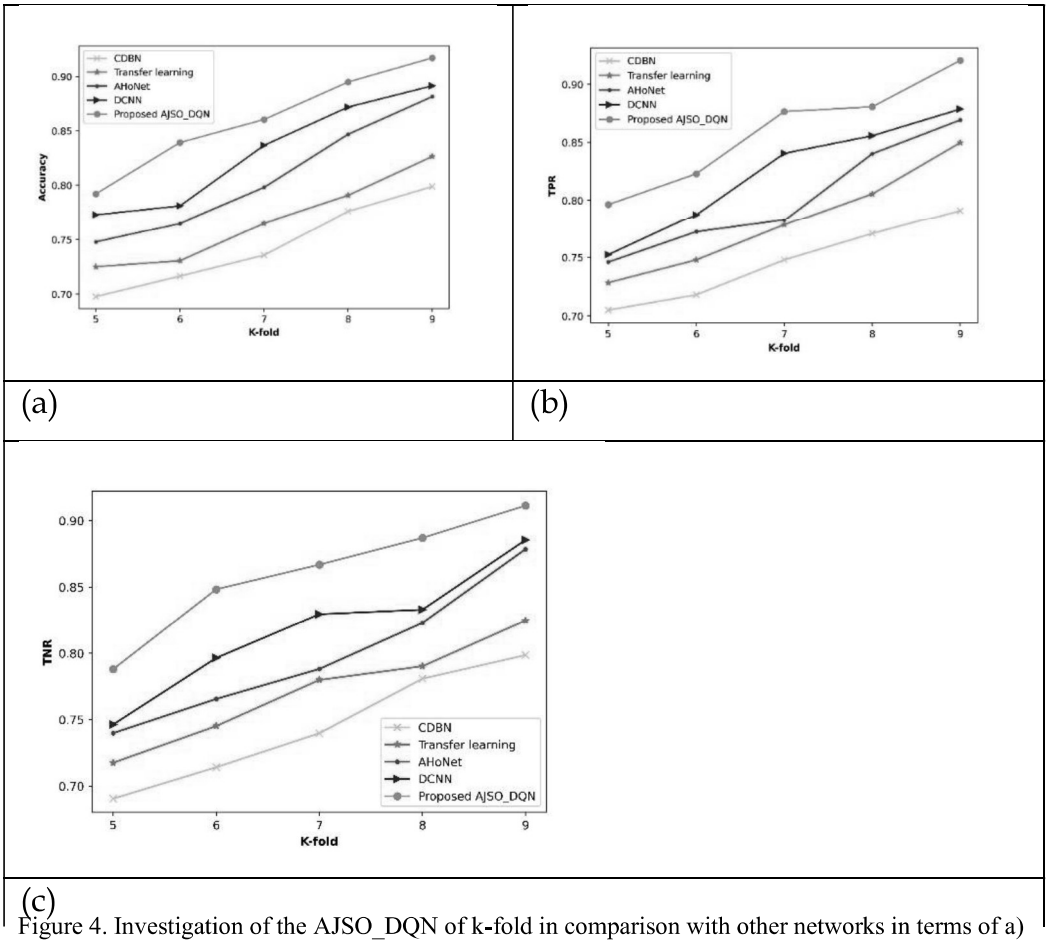

Figure 4. Investigation of the AJSO_DQN of k-fold in comparison with other networks in terms of a) accuracy, b) TPR, and c) TNR

4.6.2 Assessment based on training data

By changing training data from 50% to 90%, the developed AJSO_DQN is compared to assessment procedures in Figure 5. Figure 5 a) displays an accuracy estimation of AJSO_DQN. For 90% of the data, the accuracy of AJSO_DQN was 0.911, while the accuracy of CDBN, Transfer learning, AHoNet, and DCNN was 0.798, 0.823, 0.872, and 0.888, respectively. Notwithstanding, AJSO_DQN beat different strategies regarding exactness.An assessment of AJSO_DQN in view of TPR is displayed in Figure 5(b). AJSO_DQN had a TPR of 0.921 for 90% of the data, whereas previous methods had TPRs of 0.795 for CDBN, 0.844 for transfer learning, 0.888 for AHoNet, and 0.890 for DCNN, respectively.An estimate of the TNR is depicted in Figure 5 (c). With a TNR of 0.920, AJSO_DQN considered 90% of the data. The TNR values are 0.790, 0.842, 0.892, and 0.899 for conventional approaches for CDBN, Transfer learning, AHoNet, and DCNN.

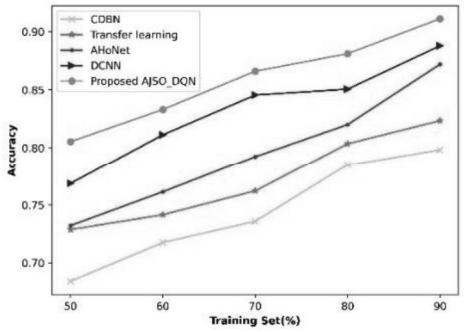

(a)

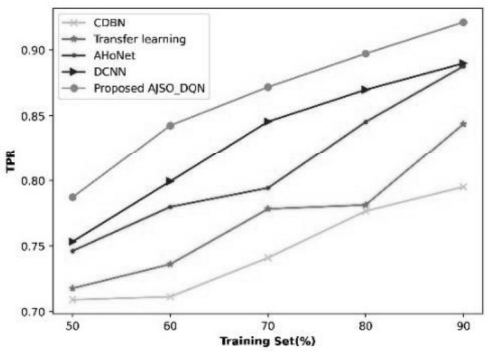

(b)

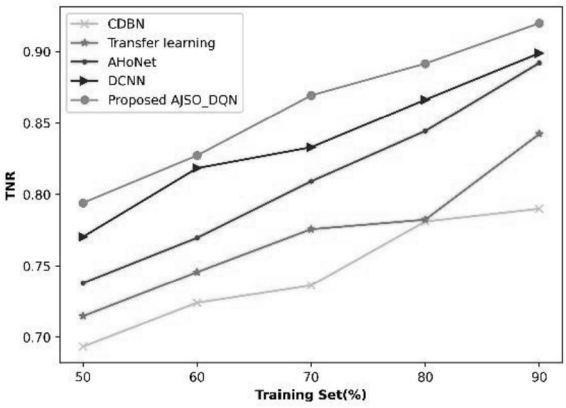

(c)

Figure 5. Comparison of the AJSO_DQN's training data with data from other networks in terms of a) accuracy, b) TPR, and c) TNR

4.7 Comparative discussion

The values of AJSO_DQN are explained in Table 1. By comparing the developed approach to the currently used methods, it can be shown from the table below that it has acquired persistent values. Using 90% of the training data, it is assumed that the established model has provided accuracy, TPR, and TNR seen as 91.7%, 92.1%, and 92.0%, respectively.

Table 1. Comparative argument of AJSO_DQN

Dataset	Metrics/Methods	CDBN	Transfer learning	AHoNet	DCNN	Proposed AJSO_DQN
K-fold	*Accuracy (%)*	79.9	82.7	88.2	89.2	91.7
	TPR (%)	79.1	85.0	86.9	87.9	92.1
	TNR (%)	79.9	82.5	87.9	88.6	91.1
Training data	*Accuracy (%)*	79.8	82.3	87.2	88.8	91.1
	TPR (%)	79.5	84.4	88.8	89.0	92.1
	TNR (%)	79.0	84.2	89.2	89.9	92.0

5. Conclusion

This paper proposes an optimisation-based deep learning technique for the breast cancer detection from histopathological images. Initially, the image from the figshare dataset is sent to the pre-processing phase. In the pre-processing stage, a median filter is employed to eliminate the noises from images. Furthermore, the pre-processed images are sent to the segmentation process. The FLICM algorithm is used to segment blood cells. Then, the features, including SURF, area, shape, and diameter features are extracted. Finally, the breast cancer detection is performed by the AJSO_DQN, in which DQN is trained by the AJSO algorithm. The performance of the proposed method is analysed using several metrics. It has been demonstrated that the developed method has high accuracy, TPR, and TNR of 91.1%, 92.1%, and 92%, respectively. In the future, huge databases will be used to check the performance of the breast cancer classification.

References

[1]. Mohanakurup, V., ParambilGangadharan, S.M., Goel, P., Verma, D., Alshehri, S., Kashyap, R. and Malakhil, B., "Breast cancer detection on histopathological images using a composite dilated Backbone Network", Computational Intelligence and Neuroscience, 2022.

[2]. Ahmad, N., Asghar, S. and Gillani, S.A., "Transfer learning-assisted multi-resolution breast cancer histopathological images classification", The Visual Computer, vol.38, no.8, pp.2751-2770, 2022.

[3]. Zou, Y., Zhang, J., Huang, S. and Liu, B., "Breast cancer histopathological image classification using attention high-order deep network", International Journal of Imaging Systems and Technology, vol.32, no.1, pp.266-279, 2022.

[4]. Burcak, K.C., Baykan, O.K. and Uguz, H., "A new deep convolutional neural network model for classifying breast cancer histopathological images and the hyperparameter optimisation of the proposed model", The Journal of Supercomputing, vol.77, pp.973-989, 2021.

[5]. Maheshan, C.M. and Prasanna Kumar, H., "Performance of image pre-processing filters for noise removal in transformer oil images at different temperatures", SN Applied Sciences, vol. 2, pp.1-7, 2020.

[6]. Krinidis, S. and Chatzis, V., "A robust fuzzy local information C-means clustering algorithm", IEEE transactions on image processing, vol.19, no.5, pp.1328-1337, 2010.

[7]. Bay, H., Ess, A., Tuytelaars, T. and Van Gool, L., "Speeded-up robust features (SURF)", Computer vision and image understanding, vol.110, no.3, pp.346-359, 2008.

[8]. Sasaki, H., Horiuchi, T. and Kato, S., "A study on vision-based mobile robot learning by deep Q-network", In Proceedings of 2017 56th annual conference of the society of instrument and control engineers of Japan (SICE), pp. 799-804, IEEE, 2017.

[9]. Chou, J.S. and Molla, A., "Recent advances in use of bio-inspired jellyfish search algorithm for solving optimisation problems", Scientific Reports, vol. 12, no. 1, pp.19157, 2022.

[10]. Hu, C., Sun, X., Yuan, Z. and Wu, Y., "Classification of breast cancer histopathological image with deep residual learning", International Journal of Imaging Systems and Technology, vol.31, no.3, pp.1583-1594, 2021.

[11]. Jiang, Y., Chen, L., Zhang, H. and Xiao, X., "Breast cancer histopathological image classification using convolutional neural networks with small SE-ResNet module",PloS one, vol.14, no.3, pp. e0214587, 2019.

[12]. He, K., Zhang, X., Ren, S. and Sun, J., "Deep residual learning for image recognition", In Proceedings of the IEEE conference on computer vision and pattern recognition, pp.770-778, 2016.

[13]. Figshare dataset is taken from, "https://figshare.com/articles/brain_tumour_dataset/1512427", accessed on March 2023.

[14]. Ghayumizadeh, H., Pakdelazar, O., Haddadnia, J., Rezai, R.G. And Mohammad, Z.M.,"Diagnosing breast cancer with the aid of fuzzy logic based on data mining of a genetic algorithm in infrared images", 2012.

[15]. Shadi Momtahen, Maryam Momtahen, Ramani Ramaseshan, and Farid Golnaraghi, "A Machine Learning Approach: NIR Scattering Data Analysis for Breast Cancer Detection and Classification," In proceedings of the IEEE 1st Industrial Electronics Society Annual On-Line Conference (ONCON), Kharagpur, India, 2022.

[16]. Yanan Shao, Hoda S. Hashemi, Paula Gordon, Linda Warren, Jane Wang, Robert Rohling, and Septimiu Salcudean, "Breast Cancer Detection Using Multimodal Time Series Features From Ultrasound Shear Wave Absolute Vibro-Elastography," IEEE Journal of Biomedical and Health Informatics, vol. 26, no. 2, pp. 704 - 714, February 2022.